



Crack propagation behavior of inhomogeneous laminated Ti–Nb metal–metal composite

Wen-juan CHENG¹, Yong LIU¹, Da-peng ZHAO², Bin LIU¹, Yan-ni TAN¹, Xiao-gang WANG³, Han-chun TANG¹

1. State Key Laboratory of Powder Metallurgy, Central South University, Changsha 410083, China;

2. College of Biology, Hunan University, Changsha 410082, China;

3. State Key Laboratory of Advanced Design and Manufacturing for Vehicle Body, Hunan University, Changsha 410082, China

Received 9 December 2018; accepted 5 May 2019

Abstract: In order to investigate the real-time cracking behavior of each component of a composite with strong interfacial bonding among lamellae, Ti–18Nb (at.%) composite was prepared by spark plasma sintering (SPS), followed by hot-rolling, annealing, and quenching. The microstructure and mechanical properties were characterized by scanning electron microscopy (SEM), energy dispersive spectroscopy (EDS), micro-region X-ray diffractometry (MRXRD), nanoindentation, and in-situ scanning electron microscopy tensile testing. The results show that the Ti–18Nb consists of Ti-enriched, diffusion and Nb-enriched zones, and the sharp Nb gradient across different zones leads to inhomogeneous distribution of phase and mechanical properties. A remarkable finding is that the diffusion zones not only enable the cooperative deformation between the brittle Ti-enriched zones and the ductile Nb-enriched zones but also act as the crack-arresters to prevent the local cracks in the Ti-enriched zones from further propagating across the composite.

Key words: Ti–Nb metal–metal composite; laminated microstructure; in-situ SEM tensile testing; fracture toughness; crack propagation behavior

1 Introduction

Developing strong and ductile metallic materials is usually a great challenge because the strength and ductility are mutually exclusive in most cases [1]. One of the effective strategies is to achieve inhomogeneous microstructures [2–6]. Many researchers reported better mechanical performance of the multi-layer-structured composites compared with the materials with homogeneous structures [7]. The key advantage of these composites is that the strength and the ductility can be well tailored by adjusting the microstructure parameters [8,9]. For instance, a laminated Cu/Al composite exhibited better tensile properties than either of the matrix [10]. A Cu/Cu laminated composite showed double elongation than the cold-rolled Cu without decreasing in strength [11]. However, the relatively poor interfacial bonding usually limits the further

improvement in the mechanical properties. The modulus mismatch of each component usually leads to strong stress/strain heterogeneity in the interface, and then the delamination of insufficient metallurgical bonding between adjacent lamellae would occur and leads to the premature failures of the materials [12]. Besides, the interfacial strength is also vital to cracking-resistance performance [13]. Consequently, the overall properties of composites can be further enhanced by introducing tough lamellae having strong bonding with the matrix.

The understanding of the fracture mechanism will provide useful insight into the strengthening mechanisms of the composite with novel structures. However, previous research was mainly focused on cracking performance on a macro-scale. In fact, the component would interact with each other during deformation. Recently, the in-situ scanning electron microscopy (SEM) mechanical testing system allows observing the deforming material surface on a micro-scale [14]. In this

Foundation item: Project (51625404) supported by the National Natural Science Foundation for Distinguished Young Scholar of China; Projects (51604104, 51504295) supported by the National Natural Science Foundation of China

Corresponding author: Yong LIU, Tel: +86-731-88836939, E-mail: yonliu@csu.edu.cn; Da-peng ZHAO, Tel: +86-731-88822606, E-mail: dpzhaoh@hnu.edu.cn
DOI: 10.1016/S1003-6326(19)65096-X

work, the in-situ experimental means can be used to record the complete process of crack initiation and propagation, and reveal the microstructural evolution and surface morphology change, which is beneficial to understanding the influence of bonding interfacial lamellae on the deformation/fracture behavior of the composites.

Spark plasma sintering (SPS) is a novel sintering method and can obtain full densification based on the electrical spark discharge phenomenon in a few minutes [15]. SPS technique uses a low voltage, high density pulse current and uniaxial pressure to achieve fast densification. The applied pulse discharge contributes to particle surface activation and increased diffusion rates, which enhances the sinterability of powders. At the same time, external pressure is necessary to achieve low porosity. The current can enhance the mass transportation through electron-migration, point defect generation and enhanced defect mobility. This is beneficial to forming a well-bonded interface between different powders without obvious grain coarsening [16]. Besides, considering the infinite solubility of Nb in Ti [17], the Ti–Nb system seems suitable for architecting a laminated structure with good interfacial bonding. SPS is a suitable method to produce the multi-layered Ti–Nb metallic composites.

Here, a multi-layered Ti–18Nb (at.%) metal–metal composite (MMC) was produced via SPS followed by hot-rolling, annealing, and water quenching. The in-situ SEM tensile testing was adopted to investigate the real-time cracking behavior of the inhomogeneous zones in the MMC and get a further understanding of the relationship between the interface status and performance. Besides, the influence of the inhomogeneous microstructure on the mechanical behaviors of different zones is also discussed. The results may provide a useful guideline on designing microstructure and improving the mechanical properties of composites.

2 Experimental

Ti–18at.%Nb MMC was fabricated by blending elemental Ti powders ($\leq 75 \mu\text{m}$, 99.9% purity, prepared by gas atomization technique) and Nb powders ($\leq 45 \mu\text{m}$, 99.9% purity, prepared by hydrogenation dehydrogenation technique, supplied by Qinghe Xinbao Alloy Material Co., Ltd.). Then, the mixed powders were consolidated into cylindrical billets with the same dimension (60 mm in diameter and 9 mm in height) using SPS, and sintered at 1200 °C under vacuum (5 Pa) and a uni-axial pressure of 20 MPa for 10 min. Afterwards, the billet samples were hot-rolled with a height reduction of 72% at 850 °C. The specimens were

then wire-electrode cut and annealed at 850 °C for 30 min in an evacuated quartz tube, followed by water quenching to room temperature.

Phase constitution of the MMC was characterized by a micro-region X-ray diffraction (MRXRD) analyzer (Rigaku Rapid IIR) with a Cu K_{α} radiation operated at 40 kV and 250 mA at room temperature at a step of 0.045°. Optical microscopy (OM, Leica), and scanning electron microscopy (SEM, FEI Quanta FEG 250) equipped with an energy dispersive spectroscopy (EDS) were used for microstructural examination and compositional analysis.

The microhardness and elastic modulus were measured by an IBIS nanoindentation tester, using a maximum load of 200 mN. The in-situ mechanical testing system of SHIMADZU (Model SEM-SERVO PULSER, equipped with a JSM-IT100 SEM), allowing the real-time observation on the deformation material surface with high resolution, was applied for the fracture test. The geometrical dimensions of the in-situ tensile sample are shown in Fig. 1. Then, the cycle load was applied to the sample to prepare a fatigue pre-crack at the notch tip with the length of 2 mm. The fracture test was performed at a strain rate of $1 \times 10^{-4} \text{ s}^{-1}$. The crack tip deformation process in different zones and the propagation path were observed and recorded. The crack-tip-opening angle (CTOA) is usually employed to evaluate the cracking resistance and fracture toughness, which can be estimated through the geometrical change of the crack surfaces in the recorded SEM images. The measuring method of CTOA was introduced in detail in Ref. [14].

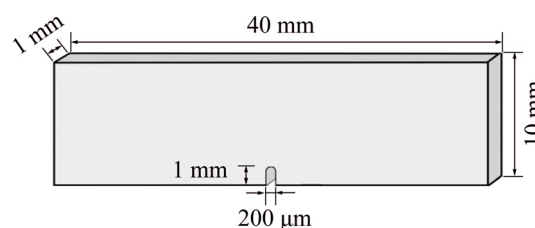


Fig. 1 Geometrical dimensions of in-situ tensile sample for fracture test

3 Results and discussion

3.1 Microstructures

Figure 2 shows the microstructure and phase constitutions of the Ti–18Nb MMC. Figure 2(a) depicts a typical rolling microstructure of the MMC with laminated dark, white and grey zones. As shown in Figs. 2(b) and (c), the compositional profile reveals that the dark, the white, and the grey zones are Ti-enriched, Ti–Nb diffusion and Nb-enriched zones, respectively. The gradient Nb distribution should be mainly attributed

to the SPS process. ZHAO et al [17] reported that the minimum sintering temperature for complete homogenization of powder-metallurgy-processed Ti–Nb alloys should be around 1300 °C. Consequently, the low sintering temperature and short time of the SPS process in this work can lead to the sharp composition gradient across the three types of zones. Further MRXRD results (Fig. 2(d)) show that the Ti-enriched and the Nb-enriched zones mainly consist of $\alpha/\alpha'+\alpha''$ phase and β/Nb phase, respectively. While, the Ti–Nb diffusion zones are composed of β/Nb phase and martensite. The phase distribution of a Ti–Nb system depends on the Nb

content and the fabrication processes [18]. The α' and α'' martensites form upon quenching from β phase with Nb content of ≤ 6 at.% and 6–25.5 at.%, respectively. So, it is reasonable that the Ti-enriched zones mainly consist of α' and α'' phase. Higher Nb content leads to retained β phase [19], so there is a high amount of β phase in the diffusion zones.

3.2 Mechanical behavior

Figure 3 shows the microhardness and elastic modulus of the three types of zones assessed from nanoindentation. The microhardness of the Nb-enriched

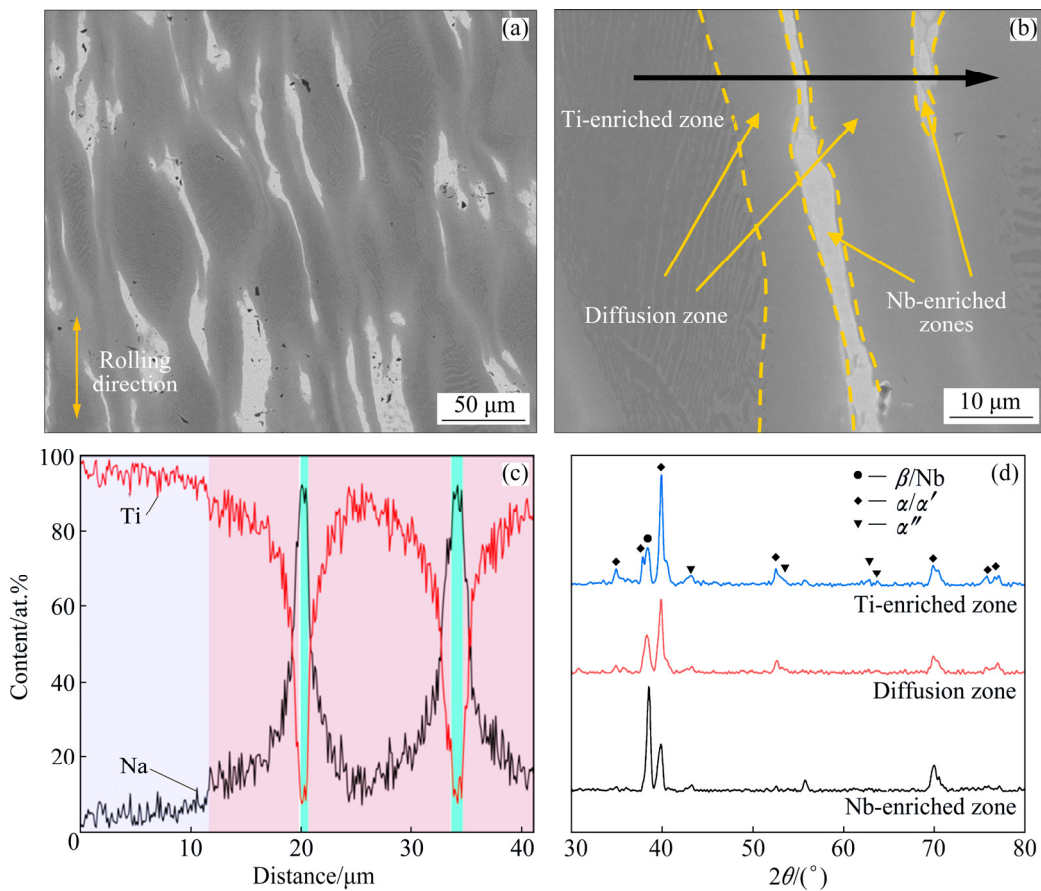


Fig. 2 SEM image (a), EDS line scanning (b, c) and MRXRD (d) of Ti–18Nb MMC

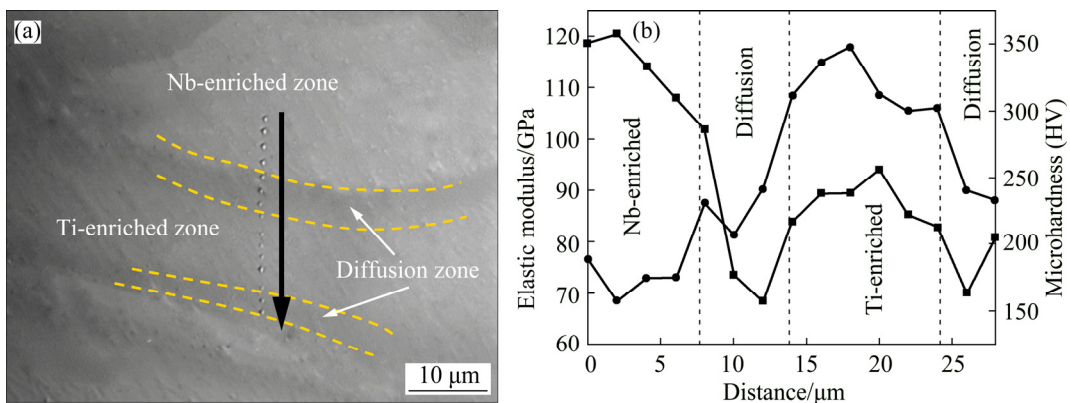


Fig. 3 Optical image (a), elastic modulus and microhardness (b) of nanoindentation points on Ti–18Nb MMC

zones is almost half that of the Ti-enriched zones, suggesting a higher strength of the latter. In the diffusion zones, the microhardness significantly increases with lower Nb content. The elastic modulus of the diffusion zones is considerably lower than that of the Ti-enriched zones (~90 GPa) and the Nb-enriched zones (100–120 GPa). The lowest value of around 65 GPa is observed in the area with moderate Nb content.

Owing to the significant influence of Nb content on the elasticity and strength of Ti–Nb alloys [20], different mechanical behaviors among three types of zones should be attributed to the sharp gradient distribution of Nb in these zones. According to ASTM B393 and ASMT F67 [21], Nb shows significantly lower yield strength than Ti, so it is reasonable that the Nb-enriched zones exhibit the lowest microhardness. Besides, the solution strengthening effect of 5–10 at.% Nb can significantly increase the hardness of the Ti-enriched zones. The diffusion zones (composed of mainly β phase) show lower microhardness than Ti-enriched zones (mainly consisting of martensite). Pure Ti shows slightly higher elastic modulus than pure Nb at room temperature (110 GPa for pure Ti [22] and 104 GPa for pure Nb [23]). However, The introduction of 5–50 at.% Nb into Ti can significantly lower elastic modulus [24], so

the diffusion zones exhibit the lowest modulus due to the low modulus β phase in Ti alloys. In contrast, low amount of Ti in Nb alloys does not significantly change the mechanical properties [25], so the high elastic modulus and low hardness of the Nb-enriched zones should be similar to those of pure Nb.

Figure 4 presents a successive of SEM images showing the fracture path during the in-situ tensile test. Figure 4(a) shows that the initial pre-crack is in the closed state before the tensile test, and the tip lies in a Ti-enriched zone. The pre-crack starts to open with a slight gap and propagates into the adjacent diffusion zone at the beginning of the tensile test (Fig. 4(b)). In the diffusion zone, the crack extension Δa does not show significant change with increasing strain, but the crack opening becomes apparent (Fig. 4(c)). At a higher magnification, massive slip bands firstly emerge around the crack tip within the diffusion and the Nb-enriched zones. As the loading further increases, the crack tip moves into the Nb-enriched zones and appears blunted (Fig. 4(d)). In the Ti-enriched zones in front of the main crack, the initiation of microcracks (e.g., Microcrack A) perpendicular to the tensile direction suggests poor ductility. Figure 4(e) shows a zigzag propagation path of the main crack in the diffusion and Nb-enriched zones,

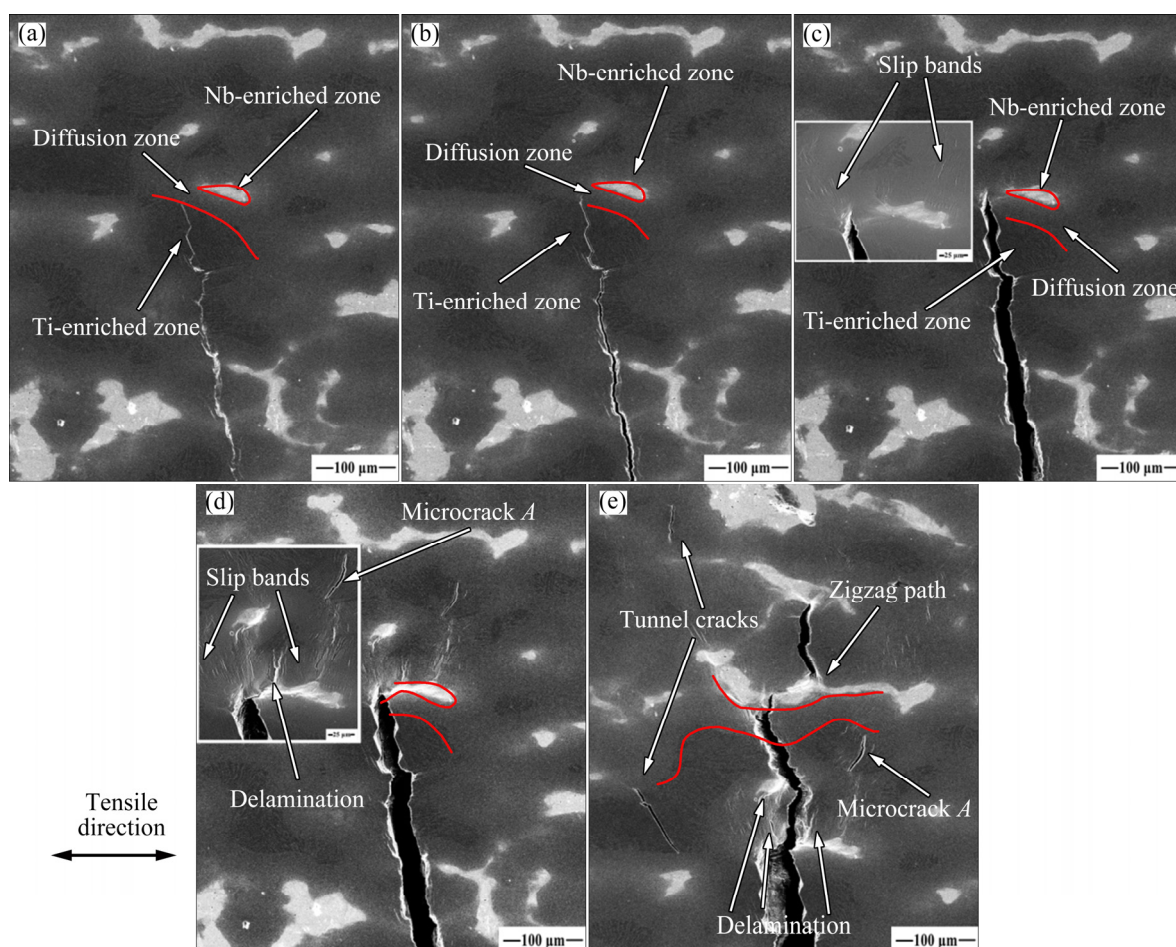


Fig. 4 In-situ SEM images of dynamic process of crack propagation at different strains: (a) 0; (b) 0.5%; (c) 1.6%; (d) 1.9%; (e) 2.2%

and there is delamination between two different zones at the edge of the main crack. The crack propagation prefers “trans-zonal” to “inter-zonal”, indicating the good interfacial bonding among the three types of zones. It is important to note that Microcrack *A* does not propagate further in Fig. 4(e).

Figure 5 reveals the significantly higher CTOA of the diffusion and the Nb-enriched zones than that of the Ti-enriched zones, suggesting the lower fracture toughness of the latter. The results are consistent with the mechanical performance observed from in-situ SEM images. Such a difference in toughness should be mainly attributed to the brittle martensite and the ductile β /Nb phase in various zones.

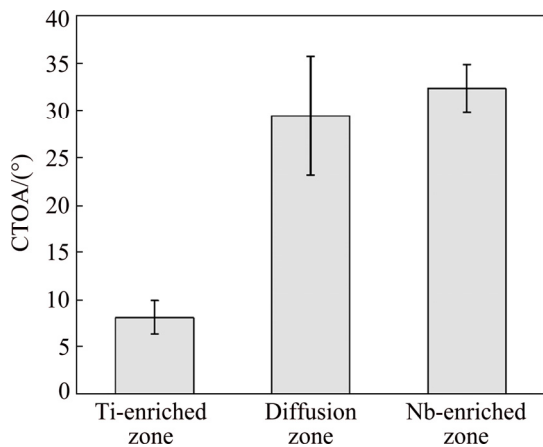


Fig. 5 CTOA of different zones in in-situ tensile fracture test

The stress intensity of the three types of zones inevitably differs from each other due to the mismatch in elastic modulus [13]. However, in this work, the strong metallurgical bonding among the zones prevents the formation of interfacial delamination. The low stiffness and high toughness of the diffusion zones provide

sufficient capacity for elastic and plastic deformation, also contributing to the cooperative deformation between the Ti-enriched and the Nb-enriched zones, which is able to maintain the overall uniform deformation for the whole material [26]. As shown in Fig. 6, when applying load on the tensile sample, the closed fatigue pre-crack begins to open and propagate perpendicular to the tensile direction. The crack path in Ti-enriched zones is thin and sharp, which is consistent with the acicular structure of the bright α' martensite phase. As the load increases, the stress concentration at the crack tip induces plastic deformation in the adjacent diffusion and the Nb-enriched zones. The slip bands occur in these two types of zones, which show higher toughness due to the softer β phase and Nb phase. When the crack tip moves into these two types of zones with much higher toughness, it becomes blunt, leading to considerable stress relaxation. Enhanced stress is needed for further crack propagation, so the tough zones also act as crack arresters. Then, there is a short delay of crack propagation until the crack growth driving force accumulates to a certain level or the crack turns to a direction easy to propagate. As a result, there are some small delaminations between two adjacent zones to relieve stress when the crack is blunt, or the crack shows a deflection. On the contrary, the harder Ti-enriched zones exhibit poor plastic deformation capability, so the tunnel cracks form in the Ti-enriched zones ahead of the crack tip at the same time. The microcracks, tunnel cracks, delamination and blunting are all beneficial to enhancing fracture toughness of the composite [27]. Besides, the tortuous fracture path in the diffusion and the Nb-enriched zones requires higher driving force and indicates the high fracture energy consumed during the crack propagation, which can probably contribute to high fracture toughness of the Ti–18Nb MMC.

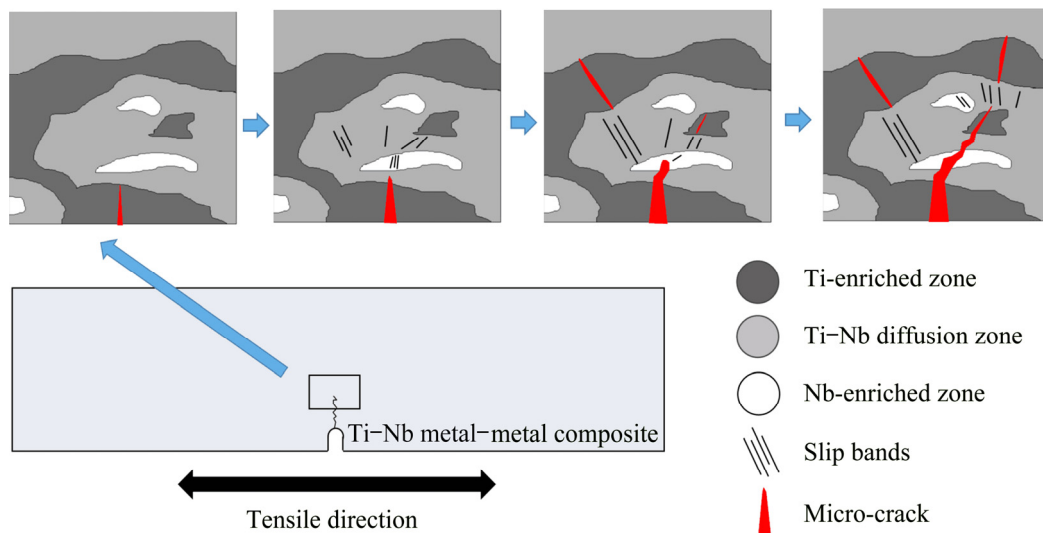


Fig. 6 Schematic diagram of crack propagation during deformation of Ti–18Nb MMC

4 Conclusions

(1) The Ti–18Nb MMC shows an inhomogeneous microstructure, consisting of Ti-enriched, diffusion and Nb-enriched zones. The high Nb gradient in the composite leads to different phase constitutions, and thus different mechanical properties of the three types of zones. The martensite should be responsible for the low toughness of the Ti-enriched zones, while the diffusion and the Nb-enriched zones, mainly composed of β /Nb phase, are much tougher.

(2) During deformation and fracture growth, owing to the low elastic modulus and the high toughness of the diffusion zones as well as the strong interfacial bonding, the three types of zones deform cooperatively. The propagation of the microcracks initiating within the Ti-enriched zones is strongly inhibited by the diffusion and the Nb-enriched zones. The crack tip blunting effect and the tortuous crack propagation path in the diffusion and Nb-enriched zones suggest an enhanced fracture toughness of the MMC compared with traditional metallic materials.

References

- [1] LU K, LU L, SURESH S. Strengthening materials by engineering coherent internal boundaries at the nanoscale [J]. *Science*, 2009, 324: 349–352.
- [2] WU X L, JIANG P, CHEN L, ZHANG J F, YUAN F P, ZHU Y T. Synergetic strengthening by gradient structure [J]. *Materials Research Letters*, 2014, 2: 185–191.
- [3] LIU Qing, QI Fa-gong, DING Hai-min, FAN Xiao-liang, YUE Ying. Distribution of stress and strain between adjacent particles in particulate reinforced metal matrix composites [J]. *Transactions of Nonferrous Metals Society of China*, 2018, 28: 2314–2323.
- [4] HUANG L J, GENG L, PENG H X. Microstructurally inhomogeneous composites: Is a homogeneous reinforcement distribution optimal? [J]. *Progress in Materials Science*, 2015, 71: 93–168.
- [5] LI Chun-hong, QIU Ri-sheng, LUAN Bai-feng, HE Wei-jun, LI Zhi-qiang. Hot deformation and processing maps of as-sintered CNT/Al-Cu composites fabricated by flake powder metallurgy [J]. *Transactions of Nonferrous Metals Society of China*, 2018, 28: 1695–1704.
- [6] FANG Meng, HU Ling, YANG Lei, SHI Chang-dong, WU Yu-cheng, TANG Wen-ming. Electroless plating and growth kinetics of Ni-P alloy film on SiC_p/Al composite with high SiC volume fraction [J]. *Transactions of Nonferrous Metals Society of China*, 2016, 26: 799–805.
- [7] LEYENS C, PETERS M. Titanium and titanium alloys [J]. *China Surface Engineering*, 2003, 23: 1–513.
- [8] HUANG L J, GENG L, PENG H X, ZHANG J. Room temperature tensile fracture characteristics of in situ TiB_w/Ti6Al4V composites with a quasi-continuous network architecture [J]. *Scripta Materialia*, 2011, 64: 844–847.
- [9] JIAO Y, HUANG L J, DUAN T B, WEI S L, KAVEENDRAN B, GENG L. Controllable two-scale network architecture and enhanced mechanical properties of (Ti₃Si₃+TiB_w)/Ti6Al4V composites [J]. *Scientific Reports*, 2016, 6: 32991–33000.
- [10] WANG T, LI S, REN Z, HAN J, HUANG Q. A novel approach for preparing Cu/Al laminated composite based on corrugated roll [J]. *Materials Letters*, 2019, 234: 79–82.
- [11] LIU H S, ZHANG B, ZHANG G P. Enhanced toughness and fatigue strength of cold roll bonded Cu/Cu laminated composites with mechanical contrast [J]. *Scripta Materialia*, 2011, 65: 891–894.
- [12] LIU B X, HUANG L J, KAVEENDRAN B, GENG L, CUI X P, WEI S L, YIN F X. Tensile and bending behaviors and characteristics of laminated Ti-(TiB_w/Ti) composites with different interface status [J]. *Composites Part B: Engineering*, 2017, 108: 377–385.
- [13] WU Hao, FAN Guo-hua, HUANG Meng, GENG Lin, CUI Xi-ping, XIE Hong-lan. Deformation behavior of brittle/ductile multilayered composites under interface constraint effect [J]. *International Journal of Plasticity*, 2017, 89: 96–109.
- [14] LI W P, WANG X G, LIU B, FANG Q H, JIANG C. Fracture mechanisms of a Mo alloyed CoCrFeNi high entropy alloy: In-situ SEM investigation [J]. *Materials Science and Engineering A*, 2018, 723: 79–88.
- [15] KIM J, JANG G S, KIM M S, LEE J K. Microstructure and compressive deformation of hypereutectic Al–Si–Fe based P/M alloys fabricated by spark plasma sintering [J]. *Transactions of Nonferrous Metals Society of China*, 2014, 24: 2346–2351.
- [16] LI Rui-di, YUAN Tie-chui, LIU Xiao-jun, WANG Jj-wei, WU Hong, ZENG Fan-hao, ZHOU Xiang. Microstructural evolution and sintering kinetics during spark plasma sintering of Fe and Al blended powder [J]. *Transactions of Nonferrous Metals Society of China*, 2017, 27: 1594–1601.
- [17] ZHAO Da-peng, CHANG Ke-ke, EBEL T, NIE He-min, WILLUMEIT R, PYCZAK F. Sintering behavior and mechanical properties of a metal injection molded Ti–Nb binary alloy as biomaterial [J]. *Journal of Alloys and Compounds*, 2015, 640: 393–400.
- [18] ZHANG Wei-dong, LIU Yong, WU Hong, LIU Bin, CHEN Zi-jin, TANG Hui-ping. Microstructural evolution during hot and cold deformation of Ti–36Nb–2Ta–3Zr–0.35O alloy [J]. *Transactions of Nonferrous Metals Society of China*, 2016, 26: 1310–1316.
- [19] ZHAO Da-peng, CHEN Yu-kai, CHANG Ke-ke, EBEL T, LUTHRIGNER-FEYERABEND B J C, WILLUMEIT-RÖMER R, PYCZAK F. Surface topography and cytocompatibility of metal injection molded Ti–22Nb alloy as biomaterial [J]. *Transactions of Nonferrous Metals Society of China*, 2018, 28: 1342–1350.
- [20] ZHANG Wei-dong, LIU Yong, LIU Bin, LI Xiao-feng, WU Hong, QIU Jing-wen. A new titanium matrix composite reinforced with Ti–36Nb–2Ta–3Zr–0.35O wire [J]. *Materials & Design*, 2017, 117: 289–297.
- [21] AVAILABLE N. Annual book of ASTM standards [M]. ASTM, 1991.
- [22] OH I H, NOMURA N, MASAHASHI N, HANADA S. Mechanical properties of porous titanium compacts prepared by powder sintering [J]. *Scripta Materialia*, 2003, 49: 1197–1202.
- [23] LI J, ZHANG Z, WANG S, WANG Y, DAI J, ZU Y, SHA J. Densification and characterization of hot-pressed ZrC-based composite doped with Nb and CNT [J]. *Materials & Design*, 2016, 104: 43–50.
- [24] HON Yen-huei, WANG Jian-yih, PAN Yung-ning. Composition/phase structure and properties of titanium-niobium alloys [J]. *Materials Transactions*, 2003, 44: 2384–2390.

- [25] CHAN K S. Alloying effects on fracture mechanisms in Nb-based intermetallic in-situ composites [J]. *Materials Science and Engineering A*, 2002, 329–331: 513–522.
- [26] LIU H S, ZHANG B, ZHANG G P. Delaying premature local necking of high-strength Cu: A potential way to enhance plasticity [J]. *Scripta Materialia*, 2011, 64: 13–16.
- [27] LIU B X, HUANG L J, RONG X D, GENG L, YIN F X. Bending behaviors and fracture characteristics of laminated ductile-tough composites under different modes [J]. *Composites Science and Technology*, 2016, 126: 94–105.

非均质片层状结构 Ti-Nb 金属-金属复合材料的裂纹扩展行为

成文娟¹, 刘咏¹, 赵大鹏², 刘彬¹, 谭彦妮¹, 王晓钢³, 汤菡纯¹

1. 中南大学 粉末冶金国家重点实验室, 长沙 410083;
2. 湖南大学 生物学院, 长沙 410082;
3. 湖南大学 车身先进设计制造国家重点实验室, 长沙 410082

摘要: 为研究具有强界面结合的金属-金属复合材料中各组分的实时裂纹扩展行为, 通过放电等离子烧结(SPS)以及后续的热轧、热处理后淬火得到 Ti-18Nb(摩尔分数, %)金属-金属复合材料。采用扫描电子显微镜(SEM)、能谱(EDS)和微区 X 射线衍射(MRXRD)、纳米压痕以及原位 SEM 实验进行显微组织与性能表征。结果表明, 该材料由富 Ti 区、过渡区以及富 Nb 区构成, Nb 在不同区域间存在明显的成分梯度, 从而造成不同区域间相分布以及力学性能的差异。过渡区具有良好的界面结合能力, 有利于实现不同区域之间的协调变形, 局部微裂纹最先在富 Ti 区出现, 过渡区与富 Nb 区具有良好的变形能力, 对裂纹扩展有一定的阻碍作用, 从而提高材料的断裂韧性。

关键词: Ti-Nb 金属-金属复合材料; 层状显微组织; 原位扫描拉伸断裂试验; 断裂韧性; 裂纹扩展行为

(Edited by Bing YANG)